JACS
JOURNAL OF THE AMERICAN CHEMICAL SOCIETY
pubs.acs.org/JACS
Article

Metastable Ni(I)-TiO_{2-x} Photocatalysts: Self-Amplifying H_2 Evolution from Plain Water without Noble Metal Co-Catalyst and Sacrificial Agent

Marco Altomare,* Shanshan Qin, Viktoriia A. Saveleva, Zdenek Badura, Ondrej Tomanec, Anca Mazare, Giorgio Zoppellaro, Alberto Vertova, Angelo Taglietti, Alessandro Minguzzi, Paolo Ghigna, and Patrik Schmuki*

Cite This: J. Am. Chem. Soc. 2023, 145, 26122−26132

ABSTRACT: Decoration of semiconductor photocatalysts with cocatalysts is generally done by a step-by-step assembly process. Here, we describe the self-assembling and self-activating nature of a photocatalytic system that forms under illumination of reduced anatase TiO_2 nanoparticles in an aqueous Ni^{2+} solution. UV illumination creates *in situ* a $Ni^+/TiO_2/Ti^{3+}$ photocatalyst that self-activates and, over time, produces H_2 at a higher rate. *In situ* X-ray absorption spectroscopy and electron paramagnetic resonance spectroscopy show that key to self-assembly and self-activation is the light-induced formation of defects in the semiconductor, which enables the formation of monovalent nickel (Ni^+) surface states. Metallic nickel states, i.e., Ni^0, do not form under the dark (resting state) or under illumination (active state). Once the catalyst is assembled, the Ni^+ surface states act as electron relay for electron transfer to form H_2 from water, in the absence of sacrificial species or noble metal cocatalysts.

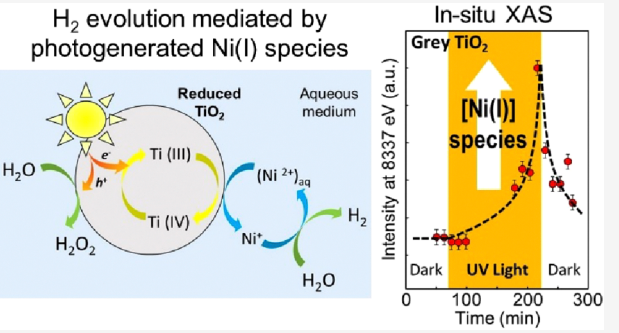

INTRODUCTION

In materials science, phenomena of self-assembly can be observed on a wide range of length scales, and many examples are relevant to create specific functional materials.[1] Some important photoinduced processes are based on self-aggregation, -formation, and -organization.[2] Such self-assembly processes that occur by "simmering in one pot for sufficient time" represent a stark contrast to the general synthesis strategies used in a chemical or materials science laboratory. In classic synthesis approaches, complex functionality is achieved by a careful step-by-step procedure that targets an optimization of each step. For example, photocatalysts are typically designed from a semiconductor that allows for light harvesting and charge carrier generation, while cocatalysts are decorated onto the semiconductor to overcome the intrinsic kinetic hindrance of many important photocatalytic reactions. In fact, from a purely thermodynamic standpoint, the position of band edges in TiO_2 can enable the reaction of H_2O into H_2, O_2, and •OH radicals as well as H_2O_2.[3−6] Nonetheless, even with the thermodynamic advantages for water splitting into H_2 and O_2, unaltered (stoichiometric) phases of TiO_2 exhibit unsatisfactory rates of H_2 evolution and undetected O_2 evolution from pure water, as well documented in the literature.[7,8] The observation that O_2 generation is less than stoichiometric or entirely absent can be ascribed not only to the sluggish kinetics of the oxygen evolution reaction (OER) in the absence of any catalysts but also to the fact that photoreduced TiO_2 tends to strongly adsorb oxygen as O_2^- or as O_2^{2-}.[9]

More generally, for many semiconductors without cocatalysts, O_2 and H_2 evolution reactions are kinetically hampered.[10−12] To overcome this limitation, noble metals such as Pt, Pd, Rh, among others, are decorated in the form of cocatalyst nanoparticles on the semiconductor surface for H_2 evolution.[13−16] To promote hole-transfer toward O_2 evolution, catalysts such as IrO_2 or RuO_2[1718] are typically used. Electron and hole transfer processes can also be facilitated using sacrificial agents.[19,20]

In recent years, research on cocatalysts increasingly focused on replacing "costly" noble metals with more economic alternatives, such as sulfides or phosphides[21−24] of various transition metals, or their alloys.[25−29] Among the latter, particularly Ni and its alloys have attracted wide interest, particularly for the surface modification of TiO_2 and $SrTiO_3$ photocatalysts.[30−34] The CB and VB edges of TiO_2 are

Received: July 30, 2023
Revised: November 8, 2023
Accepted: November 9, 2023
Published: November 20, 2023

https://doi.org/10.1021/jacs.3c08199
J. Am. Chem. Soc. 2023, 145, 26122−26132

positioned at −0.5 and +2.5 eV, respectively,[4] while the CB and VB edges of $SrTiO_3$ lay at about −0.8 and +2.5 eV, respectively[35] (vs SHE, pH 7). The electrochemical potential of the Ni^{2+}/Ni redox couple is −0.64 V (vs SHE, pH 7). In this framework, Ni has been found to be bifunctional, i.e., it can serve in the metallic form as cocatalyst for H_2 evolution and in the oxidized form (oxyhydroxide) as cocatalyst for O_2 generation.[35] Some reports suggest that Ni oxide or hydroxide placed on various semiconductors can be reduced to metallic Ni by photogenerated conduction band (CB) electrons.[35] However, there are controversial results on the photocatalytic reduction of Ni^{2+} species from solution to metallic Ni on a photocatalyst surface. Reduction of Ni^{2+} to metallic Ni has been reported for cases where holes in the illuminated semiconductor are rapidly consumed by a hole scavenger (e.g., methanol, ethanol, etc.).[36,37] We confirmed this in previous work using *in situ* X-ray absorption spectroscopy (XAS) to study Ni-, Cu-, and NiCu-modified TiO_2.[38] For Ni-modified $SrTiO_3$, in pure water, it has been reported that photocarrier transfer may lead to disproportionation reactions forming both Ni and NiO_x sites[35] or Ni/NiO_x core−shell NPs.[39] Such NiO_x compounds or Ni/NiO_x core−shell nanostructures are then able to form a NiO_x cocatalyst for water oxidation to O_2.

In contrast to $SrTiO_3$, and some other complex semiconductors, for titanium dioxide (TiO_2), these types of reactions are not observed in plain water. That is, to achieve facile electron and hole transfer from TiO_2 to water, a noble metal cocatalyst as electron transfer mediator and an efficient hole-capturing species (such as methanol) are typically required.[19,20] However, in such cases, holes react with the sacrificial agent, and methanol photoreforming replaces the water oxidation reaction.[20] In plain water, on TiO_2, the hole transfer reaction to water and the formation of O_2 are strongly hampered.[20,40] Interestingly, some works reported that on Pt-decorated titania surfaces, a two-hole transfer to water is kinetically favored, leading to H_2O_2 rather than O_2 as reaction product.[41−44] However, also this two-hole pathway to H_2O_2 is extremely slow on a pristine TiO_2 surface, and thus the hole transfer reaction represents the real bottleneck in TiO_2 photocatalytic water splitting. In a previous study, we reported that so-called *gray* TiO_2 can provide long-lived holes that enable this two-hole pathway to H_2O_2.[4] *Gray* anatase is a form of reduced anatase TiO_2, produced by thermal hydrogenation at 500 °C, possessing defective surface structure that can promote electron and hole transfer.[45] As a result, *gray* titania decorated with metallic Ni particles was found to be an effective photocatalyst for the splitting of plain water into H_2 and H_2O_2.[4]

Here, we demonstrate a more remarkable use of *gray* anatase, that is, the *in situ* formation of a metastable photocatalyst for H_2 evolution from an aqueous Ni^{2+} solution. This takes place in the absence of sacrificial species or noble metal cocatalysts and without the formation of metallic Ni nanoparticles by photoreduction on the surface of *gray* TiO_2. *In situ* XAS and electron paramagnetic resonance (EPR) spectroscopy show light-induced formation of defects in the semiconductor combined with the formation of surface trapped monovalent Ni^+ states. We propose that such Ni^+ states act as a relay for electron transfer to form H_2 from water. This property is distinct to TiO_2 powders hydrogenated under optimal conditions, as both nonreduced *white* and over-reduced *black* titania show negligible H_2 evolution under comparable photocatalytic conditions.

RESULTS AND DISCUSSION

In a simple gastight photoreactor (quartz tube), mildly reduced anatase titania nanopowders (*gray* titania[45]) are dispersed in an aqueous 0.4 mM $NiSO_4$ solution and illuminated with UV light (UV LED, 365 nm, 100 mW cm^{-2}). Under these experimental conditions, in a few hours, an increasingly effective photocatalytic system self-assembles and a metastable state is established that produces H_2 from water. This self-activation process is illustrated in Figure 1 (see the Supplementary Information for additional experimental details and Figure S1 for further characterization of *gray* TiO_2). After switching on UV illumination, during the first few hours of illumination, only negligible amounts of H_2 can be detected (such amounts are in the range of or below the detection limit of the gas chromatograph, GC). Then, the H_2 evolution becomes evident, and after 10 h of illumination it keeps accelerating, e.g., until 72 h of illumination (at this time the UV light was turned off and the experiment was stopped). Interestingly, these self-activation and amplification phenomena take place in the absence of any sacrificial agent. We observed a similar effect in previous work where we hypothesized the formation of a monovalent nickel cocatalyst mediator.[46] Here, we prove our hypothesis by *in situ* XAS and EPR spectroscopy.

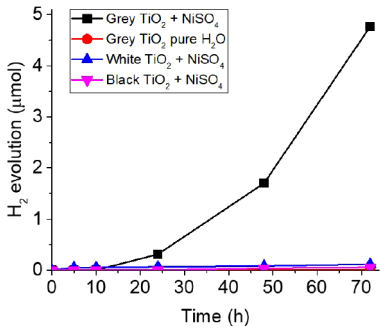

Figure 1. H_2 evolution performance: comparison of *gray* TiO_2 nanoparticles with *white* and *black* TiO_2 nanoparticles in 0.4 mM $NiSO_4{\cdot}6H_2O$ aqueous solution under illumination.

This effect is unique to *gray* anatase and cannot be observed for *white* TiO_2 (untreated anatase) or *black* TiO_2 (Figure 1). *Black* TiO_2 is a form of over-reduced (highly defective) titania produced by hydrogenation under harsh conditions (700 °C in this case).[47−50] *Black* and *gray* TiO_2 differ in the reduction treatment used to produce the materials from *white* (untreated) anatase. Consequently, the three forms of titania herein studied exhibit different density and nature of oxygen vacancies (Ti^{3+}-O_V) and, thus, different electronic properties.[45] We characterized these materials in view of their electronic and defect structure in previous work.[4,45,50−56] Unlike low temperature treatments (e.g., 500 °C) that maintain anatase as the only crystalline phase, hydrogenation at 700 °C (to form the over-reduced black TiO_2) results in a mixed anatase−rutile composition.[45] Among different "shades" of *gray* titania, i.e., thermally treated in H_2 at different reduction temperatures (300−700 °C), the powder treated at 500 °C for 1 h (*gray* TiO_2) shows the highest photocatalytic activity (shown in our previous work[46]).

Figure 1 shows that an incubation period is observed until H_2 evolution is detected in significant amounts. It is known that illumination of anatase in aqueous methanolic solutions[57] forms Ti^{3+} sites that are catalytically active for the generation of H_2.[58]

https://doi.org/10.1021/jacs.3c08199
J. Am. Chem. Soc. 2023, 145, 26122−26132

Differently, in the present work, we show how UV light can form Ti^{3+} sites that generate H_2 from plain water, i.e., in the absence of any hole scavenger, due to the presence of Ni^{2+} and via the formation of a metastable $Ni^{+}/TiO_2/Ti^{3+}$ photocatalyst (discussed below). The key role of Ni ions is evident from data in Figure 1, i.e., when comparing the H_2 evolution measured in an aqueous $NiSO_4$ solution vs Ni^{2+} free solution. Additional data on the effect of pH, temperature, nickel salt precursor, and illumination wavelength and power density on the photocatalytic H_2 evolution rate can be found in Figure S2.

A first assumption may be that photocatalytic reduction of Ni^{2+} to Ni° would occur under UV irradiation. In this case, over time, the titania would be decorated with Ni° nanoparticles that act as cocatalyst for H_2 evolution. However, we find that after illumination (even up to 10 days), no morphological trace of particle deposition can be observed on *gray* titania, neither by extensive investigations by scanning electron microscopy (SEM, Figure S3) nor by high-resolution transmission electron microscopy (HR-TEM, Figure 2a,b). Nevertheless, the presence of Ni species can be clearly detected by TEM−energy dispersive spectroscopy (TEM−EDS, Figure 2c,d), which indicates that Ni is distributed uniformly on the nanopowder. The absence of particle deposition along with the evidence of a homogeneous Ni distribution hints to atomically dispersed Ni species. Similar species are commonly encountered in single atom catalysis.[59−61]

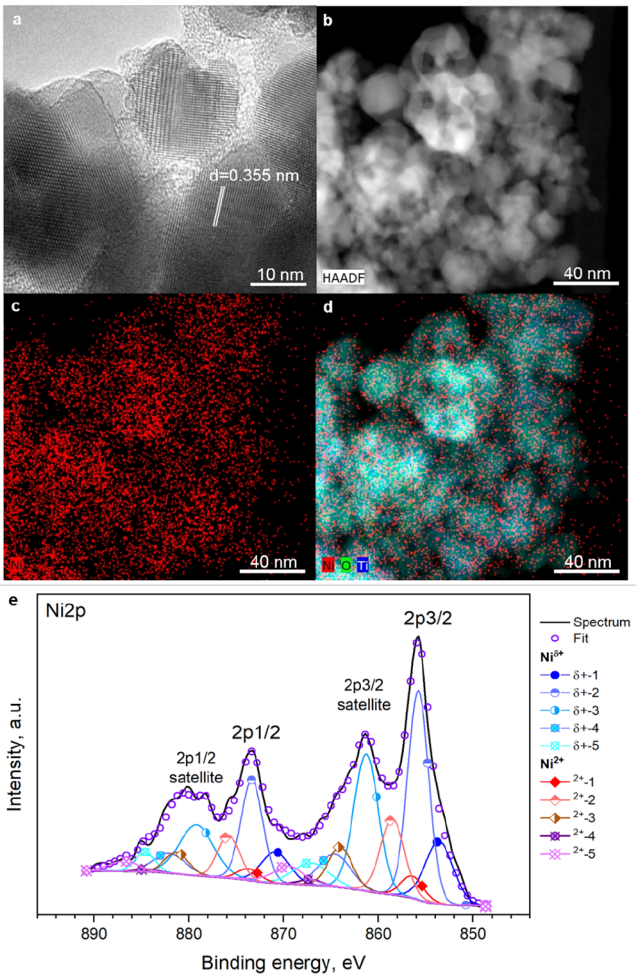

Figure 2. (a−d) *Gray* TiO_2 nanoparticles after illumination for 10 days in a 0.4 mM $NiSO_4{\cdot}6H_2O$ aqueous solution: (a) High-resolution TEM image. (b) High-angle annular dark-field imaging (HAADF). TEM−EDS elemental mappings of (c) Ni and (d) Ni, O, and Ti. (e) Peak fitting of the high resolution XPS spectrum in the Ni 2p region for the sputtered anatase TiO_2 layer (hydrogenated at 500 °C) illuminated with a 365 nm LED (100 mW cm^{-2}) for 24 h in a 0.4 mM $NiSO_4{\cdot}6H_2O$ aqueous solution.

For powder samples, the amount of Ni is below the detection limit of X-ray photoelectron spectroscopy (XPS). However, if compact, polycrystalline anatase layers produced by magnetron sputtering (on SiO_2/Si) and subsequently reduced (hydrogenation at 500 °C, 1 h) are illuminated (24 h, UV light) in a 0.4 mM $NiSO_4{\cdot}6H_2O$ aqueous solution, XPS can reveal the presence of Ni species (Figure 2e). These layers show an onset of H_2 evolution in analogy to the powder (Figure S4), and no morphological trace of photodeposited Ni particles can be observed (Figure S5). The XPS data reveal a Ni surface content of ca. 0.5 at. %, and a Ni:Ti ratio of ca. 0.04:1, indicating a low loading of Ni species (see Table S1).

The fitting of the Ni 2p XPS peak suggests the presence of Ni in various oxidations states. First, the Ni 2p consists of the Ni $2p_{3/2}$ and Ni $2p_{1/2}$ peaks at 855.9 and 873.5 eV, respectively, and with the corresponding satellite peaks at 861.3 and 879.9 eV (consistent with literature data).[62] To evaluate the chemical states of Ni, peak fitting of the Ni 2p spectrum in Figure 2e was performed. For the fitting, we used empirical fits obtained from parameters derived from standard samples typically found in literature.[63−66] The detected species include $Ni^{\delta+}$, typical of surface-coordinated Ni states, and Ni^{2+}. Consistent with SEM and TEM, no metallic Ni was detected (typical binding energy of 852.6 eV). The binding energy, full width half-maximum and percentage of the peak area of the fitted peaks comprising the $2p_{3/2}$ peak and corresponding satellite are listed in Table S2 in the Supporting Information and are consistent with literature data.[62−64] The fitted spectrum with an error below 0.5% includes the $2p_{3/2}$, $2p_{1/3}$ and satellite peaks for $Ni^{\delta+}$ (72.4%) and Ni^{2+} (27.6%). However, the *ex situ* XPS data may be affected by exposure of the sample to air due to sample removal from the electrolyte and transfer to the XPS setup. In general, this issue may affect *ex situ* characterization results.

Therefore, to clarify the self-activation mechanism and the role of Ni in the photocatalytic system, we performed *in situ* XAS experiments. Experimental details are provided in the Supporting Information. In a preliminary experiment, we studied the electrochemical reduction of a Ni(II) complex $[Ni(cyclam)]^{2+}$ in an acetonitrile-based electrolyte to obtain a reference spectrum for *in situ* formed Ni(I) species; $[Ni(cyclam)]^{2+}$ is in fact known to undergo reduction to formal Ni(I) species.[67,68] Experimental details on the synthesis and characterization of the Ni(II) complex $[Ni(cyclam)]^{2+}$ are provided in the SI. The X-ray absorption near-edge structure (XANES) spectrum of the complex at the Ni K-edge is shown in Figure 3.

We measured the spectra of the complex under open circuit potential (OCP) conditions. As a reference for Ni(II), we use here a Ni K-edge XANES spectrum of NiO. The close correspondence in energy of the edge position and the overall similarity of the spectral shapes clearly demonstrate that the $[Ni(cyclam)]^{2+}$ complex features divalent nickel centers. We then polarized the working electrode (a transparent conductive oxide-coated glass slide, FTO) at −2 V (vs Ag pseudoreference electrode), since preliminary voltametric experiments showed a one-electron reduction peak to Ni(I) at about −1.8 V[69] (see CV in Figure S6). In the Ni K-edge spectrum, a new structure at ca. 8337.1 eV appears (green arrow in Figure 3, highlighted in the

https://doi.org/10.1021/jacs.3c08199
J. Am. Chem. Soc. 2023, 145, 26122−26132

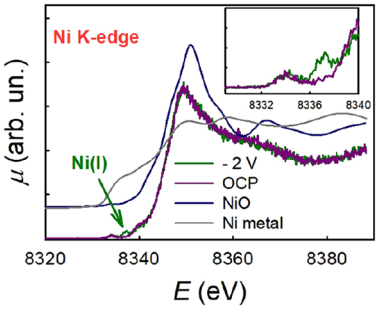

Figure 3. XANES spectra of the $[Ni(cyclam)]^{2+}$ complex at the OCP and −2 V. Ni and NiO spectra are shown as a reference for Ni(0) and Ni(II) oxidation states, shifted along the *y* axis for better clarity. Inset: pre-edge region for the $[Ni(cyclam)]^{2+}$ complex at the OCP and −2 V.

inset). We can refer to this feature as the signature of Ni(I). In addition, the spectrum at −2 V clearly indicates that Ni^0, i.e., metallic nickel, does not form.

We then performed *in situ* XAS experiments studying the different TiO_2 photocatalysts in aqueous suspensions in the presence of $NiSO_4$, both under dark conditions and under UV light illumination (i.e., under photocatalytic H_2 evolution conditions). A picture of the setup along with experimental details and can be found in Methods and Figure S7, respectively. The XANES spectra at the Ni K-edge of *gray* TiO_2 (in a 0.4 mM solution of $NiSO_4$) under different conditions are shown in Figure 4a. In the dark, the spectrum resembles that of Ni(II) hydrated ions. Figure S8 shows the Ni K-edge XANES spectrum of a 0.4 mM aqueous solution of $NiSO_4$, compared to the spectra of the same solution in the presence of black, gray, and white

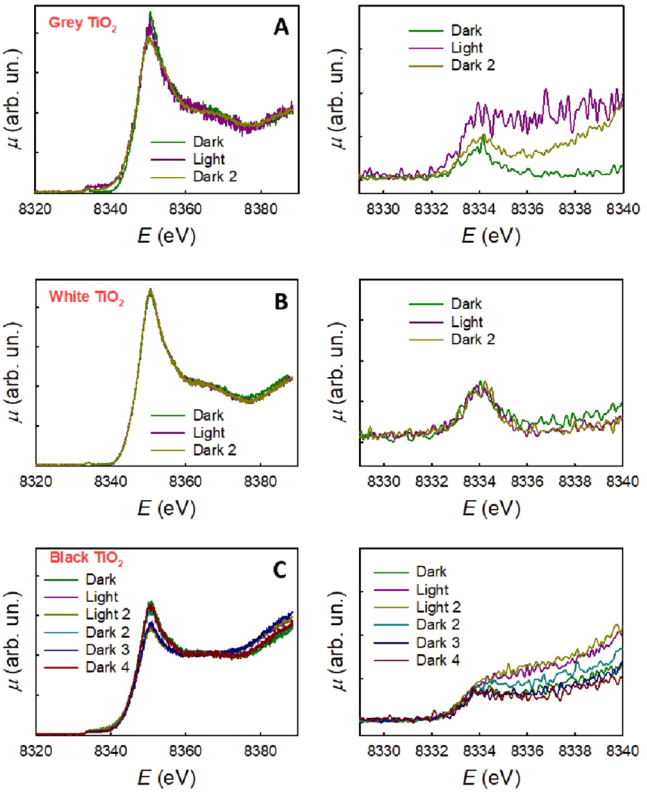

Figure 4. XANES spectra of *gray* (a), *white* (b), *and black* (c) TiO_2 in a 0.4 mM solution of $NiSO_4$ under intermittent UV light illumination. Right panels: magnified pre-edge regions.

TiO_2, all under dark conditions. The close similarity of the absorption edge position for all of the spectra confirms that the oxidation state is Ni(II) in every case. Minor differences are visible when the solution is put in contact with the different TiO_2 powders, which may be indicative of the formation of different Ni(II) species adsorbed onto the TiO_2 nanoparticles.

Upon illumination, a new broad feature appears at ca. 8336−8338 eV, and this is indicative of the formation of Ni(I). We note that this structure in the presence of TiO_2 is broader when compared to the signal obtained by electrochemical reduction of the $[Ni(cyclam)]^{2+}$ complex (Figure S9). This may be related to the fact that the Ni(I) sites are adsorbed on the TiO_2 nanoparticle surface and therefore are expected to experience significant local disorder. Note that no Ni^0, i.e., metallic nickel, could be detected, neither in the dark (resting state) nor under illumination (active state).

When the light is switched off, this structure decreases in intensity, thus confirming that the formation of Ni(I) is driven by illumination and is reversible. The fact that the Ni(I) feature at ca. 8337 eV disappears shortly after illumination indicates that such Ni(I) species are highly reactive, i.e., are short lived, according to

$$Ni^{2+} + e^- \rightarrow Ni^+_{surface} \text{ and } 2Ni^+_{surface} + 2H^+ \rightarrow H_2 + 2Ni^{2+}$$

The XANES spectra at the Ni K-edge of *white* TiO_2 in a 0.4 mM solution of $NiSO_4$ under different conditions are shown in Figure 4b. In the dark, the spectrum resembles that of Ni(II) hydrated ions, and under illumination, no difference can be detected. The same is valid for this sample in the dark after illumination. As shown in Figure 1, *white* TiO_2 shows negligible photocatalytic activity, which is now further substantiated by the fact that no Ni(I) species form, neither in the dark nor under illumination, in the case of white titania.

The XANES spectra at the Ni K-edge of *black* TiO_2 in a 0.4 mM solution of $NiSO_4$ under different conditions are shown in Figure 4c. In the dark, the spectrum shows a spectral weight in the energy region of Ni(I), and this increases upon illumination. After illumination, the original spectral shape is recovered only after a long time in the dark (ca. 3 h). These conclusions are, however, made less straightforward by the fact that, in the energy region characteristic of N(I), also Ni(0) has an increased spectral weight. Nevertheless, these results seem to indicate that defective Ti^{3+}-O_V sites in *black* TiO_2 are highly active also in the dark, and a reaction with Ni(II) aqueous ions to form surface Ni(I) species takes place also without photogeneration of charge carriers in TiO_2. Note that *black* TiO_2, as shown in Figure 1, shows negligible photocatalytic activity.

In situ time-resolved XAS data help highlight the spectral differences between the three TiO_2 samples, as shown in Figure 5. The value of the absorption intensity at 8337.1 eV, after normalization for the intensity at the main edge peak, is plotted as a function of time during the dark−light−dark cycles.

To sum up, the behavior of the three studied samples is very different. *White* TiO_2 (center) is the simplest case: both under dark conditions and under UV illumination, the formation of Ni(I) can be excluded. For *gray* TiO_2 (left) the formation of Ni(I) species requires UV illumination. The concentration of Ni(I) increases after an induction period, and decreases immediately when the illumination is switched off. The induction period resembles that observed during the photocatalytic H_2 evolution experiments (see Figure 1). *Black* TiO_2 (right), in contrast, shows the presence of Ni(I) species both in the dark and under illumination. Upon illumination, the concentration of Ni(I) increases only slightly and reaches

https://doi.org/10.1021/jacs.3c08199
J. Am. Chem. Soc. 2023, 145, 26122−26132

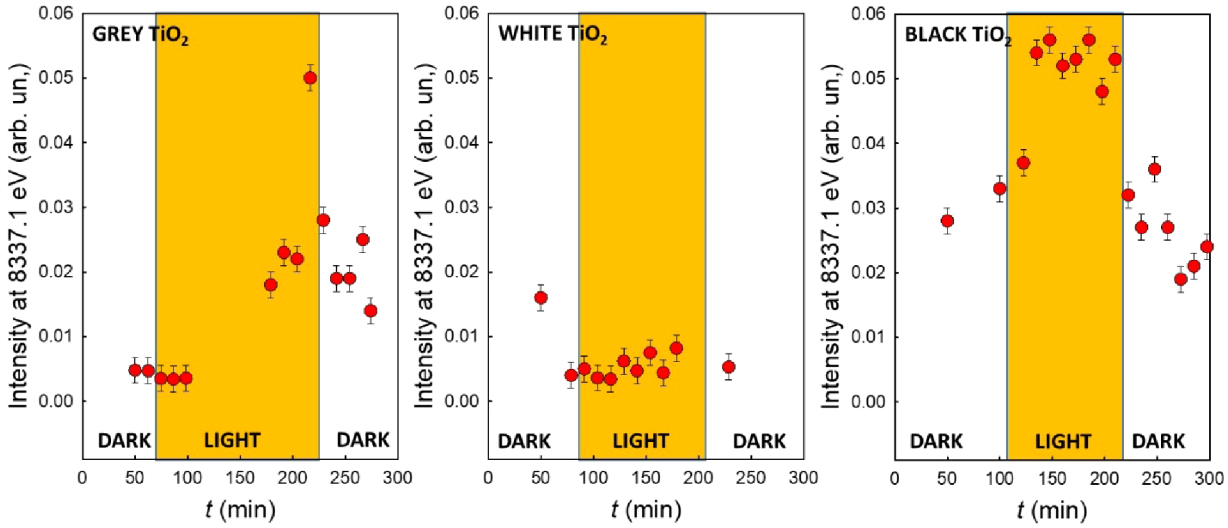

Figure 5. *In situ* time-resolved XAS data showing the trend of the absorption intensity at 8337.1 eV vs time for the different TiO_2 samples.

soon a plateau. After switching off the illumination, it returns to its initial value.

Summarizing the results of photocatalytic H_2 evolution experiments and *in situ* XAS, we observe that:

- Common to all parameter variations in photocatalytic H_2 evolution experiments with *gray* TiO_2 in aqueous $NiSO_4$ solutions (Figures 1 and S2) is that, after starting UV illumination, an incubation period is observed until H_2 is produced in detectable amounts. On the contrary, in the absence of Ni(II) salt, the H_2 generation remains negligible.
- No Ni^0, i.e., metallic nickel, can be detected, neither in the dark (resting state) nor under illumination (active state) for the tested photocatalyst.
- The XAS signal ascribed to Ni(I) species (Figure 5) increases over time under UV illumination, and so does the amount of generated H_2 detected by GC analysis (Figures 1 and S2), suggesting that the two redox processes (Ni^+ formation and H_2 evolution) are linked, and likely the formation of Ni(I) species is the first redox step, followed by subsequent H_2 generation.
- Results from our previous work[46] suggest a strong correlation between the concentration of Ni(II) salt and the H_2 generation (optimum of Ni(II) concentration 0.4 mM, as used in the present study). This can due to a trade-off between an increase in H_2 generation activity, due to a higher concentration of photoformed Ni(I) states, and a decrease in effective reaction volume, due to a higher light absorbance of the aqueous phase with increasing the Ni(II) salt concentration.

Therefore, we conclude that

- Ni(I) species, formed on *gray* TiO_2 but not on *white* TiO_2, are key to catalyze the H_2 evolution in the absence of a sacrificial agent and noble metal cocatalyst.
- The formation of Ni(I) species can be related to the presence of surface Ti^{3+} sites on TiO_2, (confirmed by in situ EPR, below) which enable the formation of monovalent nickel (Ni(I)) species. The H_2 evolution rate appears to correlate with the concentration of such surface Ni(I) species.
- To initiate the redox chain, i.e., the formation of Ni^+ active species that enable H_2 generation, needed are not only available Ni^{2+} ions in the solution but also Ti^{3+} sites at the TiO_2 surface to react with Ni^{2+} ions. It is therefore expected that the highest H_2 generation rates are achieved when the system is optimized in view of light absorption and availability of surface Ti^{3+} sites on TiO_2 and Ni^{2+} ions in the reaction phase.
- Different hydrogenation treatments (different temperatures) form in TiO_2 Ti^{3+}-O_V sites of different density, distribution, and energy, in line with *in situ* EPR results discussed below and in our previous work.[70]
- Defective Ti^{3+}-O_V structures in *black* TiO_2 are highly reactive and form Ni(I) species already in the dark. This process, however, is not reversible, indicating that Ni(I) species formed on *black* anatase are stabilized by a strong interaction with the defective oxide surface and, hence, are less reactive. Hence, such Ni(I) species are significantly less reactive toward H_2 evolution.

Note that *gray* titania provides not only an adequate surface density of Ti^{3+}-O_V sites, but also a sufficient hole transfer ability to plain water, forming hydrogen peroxide, as shown in previous own work,[4] in preliminary results in Figure S10, and discussed below along with *in situ* EPR results. This is crucial since, in the absence of efficient hole transfer, photoholes could oxidize the monovalent nickel (to Ni(II)), and this would impede the electron transfer to water for hydrogen evolution.

To validate our interpretation, we carried out *in situ* EPR experiments to investigate the effects of UV illumination on *gray* titania nanoparticles in Ni^{2+} aqueous solutions. Figure 6a (3D plot) and Figure 6d (2D plot) show *in situ* EPR resonance spectra (T = 80 K) of *gray* titania dispersed in a Ni^{2+} aqueous solution (in the absence of hole scavenger, e.g., MeOH). The sequential spectra were acquired under fast scanning conditions of the magnetic field (30 s) during a dark-light sequence (2.5 min dark followed by 27.5 min of irradiation at 325 nm, HeCd laser, power 200 mW). Under dark conditions, the recorded EPR spectra show a broad resonance signature developing in the 330−360 mT magnetic field range ($g_{avg} \approx 1.92$, see Figure 6c, blue spectrum) and two resonance signals at lower magnetic field, at g = 1.98 and g = 2.00. These signals originate from Ti^{3+} states located in different lattice positions.[50,55] The signals at g =

https://doi.org/10.1021/jacs.3c08199
J. Am. Chem. Soc. 2023, 145, 26122−26132

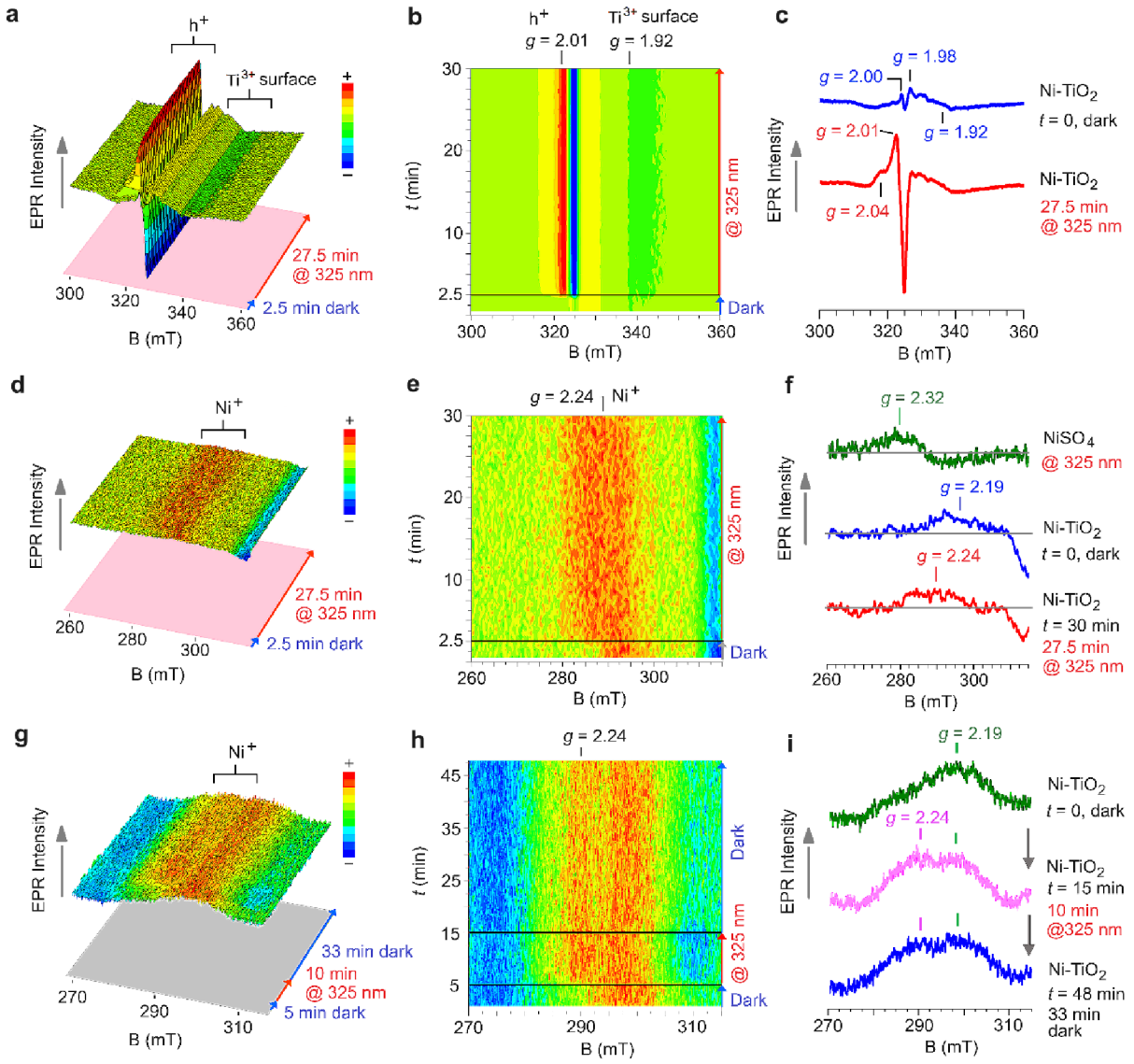

Figure 6. X-band (~9.07−9.09 GHz) light-induced electron paramagnetic resonance (LEPR) spectra recorded at $T = 80$ K of *gray* TiO_2 nanoparticles dispersed in an aqueous $NiSO_4$ solution. Panels a−f: spectra were recorded in (oxygen containing) water, with and without light irradiation. Experimental conditions: X-band frequency 9.072 GHz, 0.4 mW applied power, 1.0 mT modulation width, 30 s sweep time for each sequential spectrum, and 0.03 s time constant. Panels g−i: spectra recorded in a 20 vol % $MeOH/H_2O$ mixture (nitrogen saturated), with and without light irradiation. Experimental conditions: X-band frequency: 9.086 GHz, 1.6 mW applied power, 0.6 mT modulation width, 60 s sweep time for each sequential spectrum, and 0.03 s time constant.

2.00 corresponds to electrons trapped into oxygen vacancies, Ti^{3+}-O_V, and the resonance at $g = 1.98$ corresponds to Ti^{3+} sites formed in bulk lattice positions. The broad signature at $g_{avg} \approx 1.92$ originates from surface exposed Ti^{3+} sites.[50,54,55] Weaker resonances are detected also in the lower magnetic field region (higher g-values), around $g = 2.02-2.01$; these resonances arise from trapped holes in the form of oxygen-based radicals (e.g., $Ti-O^{\bullet}$ species).

Soon after UV illumination, several changes become evident, as shown in the 3D (Figure 6a,d) and 2D plots (Figure 6b,e): (i) the appearance of the strong hole signature at $g_1 = 2.04$ and $g_2 = 2.01$ (see Figure 6c, red spectrum), (ii) the small increase of the signal of lattice embedded Ti^{3+} ($g_{avg} = 1.92$), best resolved in the 2D plot shown in Figure 6b, and importantly (iii) the formation of a new resonance feature at $g \approx 2.24$ that can be assigned to the development of photoactive Ni^+ sites ($S = 1/2$, $3d^84s^1$) (see Figure 6d,e).

The $g \approx 2.24$ signal (see Figure 6f, red spectrum) is broad and very weak. This is due to the low concentration of Ni centers on the surface of *gray* titania along with different Ni coordination environments due to local disorder − this can explain the increase of the resonance line width. Note that before UV irradiation in the spectral range where the resonance at $g \sim 2.24$ develops, another broad signal is also detected at $g \sim 2.19$ (see the 2D plot in Figure 6e and the blue spectrum in Figure 6f). This resonance cannot arise from the presence of Ni^{2+} cations, because Ni^{2+} usually adopts the low spin state and is thus EPR silent ($S = 0$, $3d^8$). High spin state Ni^{2+}, a non-Kamer system ($S = 1$), has such large zero-field-splitting that becomes undetectable at X-band frequencies.[65] Ni^{2+} cations in water solution can be oxidized to Ni^{3+} giving an $S = 1/2$ configuration ($3d^7$) upon illumination at 325 nm, which produces EPR spectral features (Figure S11, $g_z = 2.32$ and $g_x = g_y = 2.06$ that are different than those observed here with *gray* titania in the dark or

https://doi.org/10.1021/jacs.3c08199
J. Am. Chem. Soc. 2023, 145, 26122−26132

upon illumination (see Figure 6f, blue and red spectra, respectivley). For example, a Ni^{3+}-EDTA complex ($S = 1/2$) formed in aqueous solution upon irradiation of Ni^{2+}-EDTA solutions was reported to exhibit EPR signatures at $g_z = 2.336$ and $g_x = g_y = 2.139$ (spectrum recorded at $T = 77$ K, ^{60}Co γ-source).[66] Therefore, the weak and broad resonance we observe under dark conditions at $g \sim 2.19$ can be associated with the presence on the *gray* titania of a small fraction of less reactive Ni^+ species that are strongly interacting with the defective oxide surface; such sites are already present before UV light irradiation, and form when the titania powder is suspended in the Ni salt solution. We propose that these Ni^+ species form by electron transfer from surface exposed Ti^{3+} sites to Ni^{2+} cations. It should be noted that the concentration of such Ni^+ species is rather low and just above the detection limit of EPR (a spin sensitive technique).

To gain further knowledge of the resonance signals developing in the $g = 2.2$ region and investigate the reversibility of photogeneration of Ni^+ species, light-induced electron paramagnetic resonance (LEPR) experiments were performed at $T = 80$ K for the Ni^{2+}-gray TiO_2 water suspension upon addition of a small amount of MeOH as hole scavenger (20 vol % $MeOH/H_2O$) and by using nitrogen saturated solutions. We applied a dark−light−dark sequence (5 min dark followed by 10 min of irradiation at 325 nm and then 33 min dark). Results are shown in Figure 6g (3D plot), Figure 6h (2D plot) and Figure 6i. In dark conditions at $t = 0$ min, the Ni^+ signal at $g = 2.19$ (around 300 mT) becomes more resolved (Figure 6i, olive line), showing the presence of a shoulder at a lower magnetic field (275−290 mT). This shoulder, a distinct signal at $g = 2.24$ (see Figure 6g,h, time window 5−15 min, and Figure 6i, pink spectrum), belongs to highly photoactive Ni^+ sites that are generated under UV irradiation of the sample in the EPR tube before freezing in liquid N_2. When shutting down the UV light, the signal at $g = 2.24$ slowly decays at 80 K (see Figure 6g,h, time window 16−48 min, and Figure 6i, blue spectrum) while the signal at $g = 2.19$ does not. Therefore, we conclude that the signal at $g = 2.24$ belongs to the metastable Ni^+ species, confirming the XANES results. We propose that, besides the fraction of Ni^+ centers already formed in the dark in the as prepared materials (less reactive sites), surface adsorbed Ni^{2+} cations can act as (reversible) electron acceptors as soon as UV light is switched on, forming EPR active Ni^+ species that are responsible for the photocatalytic H_2 evolution activity of *gray* TiO_2. The data point toward an electronic rearrangement that takes place between Ti^{3+} sites and adsorbed Ni^{2+} ions. Such reaction can be expressed in the form of: $Ti^{3+} + Ni^{2+} \rightarrow Ti^{4+}-Ni^+$, and therefore the Ni^{2+} centers must be either located nearby a surface exposed Ti^{3+} site or trapped in a $Ti^{3+}-Ni^{2+}$ configuration.

We also monitored by *in situ* LEPR experiments the magnetic field region where photogenerated holes and Ti^{3+} sites evolve (310−350 mT), using gray TiO_2 in Ni−H_2O/MeOH solutions. Spectra were recorded under identical conditions (5 min underthe dark followed by 10 min UV and then 33 min dark). Results are shown in Figure 7a,b (3D and 2D plots, respectively). Without the presence of dissolved oxygen, the spectra resolution is increased and allows to observe the formation of a new Ti resonance signature under light irradiation ($g = 1.997$, time 5−15 min) accompanied by the disappearance of the signal at $g = 1.987$ (Ti^{3+}). The disappearance of this signal exactly correlates with the formation of Ni^+ observed at $g = 2.24$.

Note that due to the presence of MeOH, the resonance associated with hole centers becomes much less dominant here,

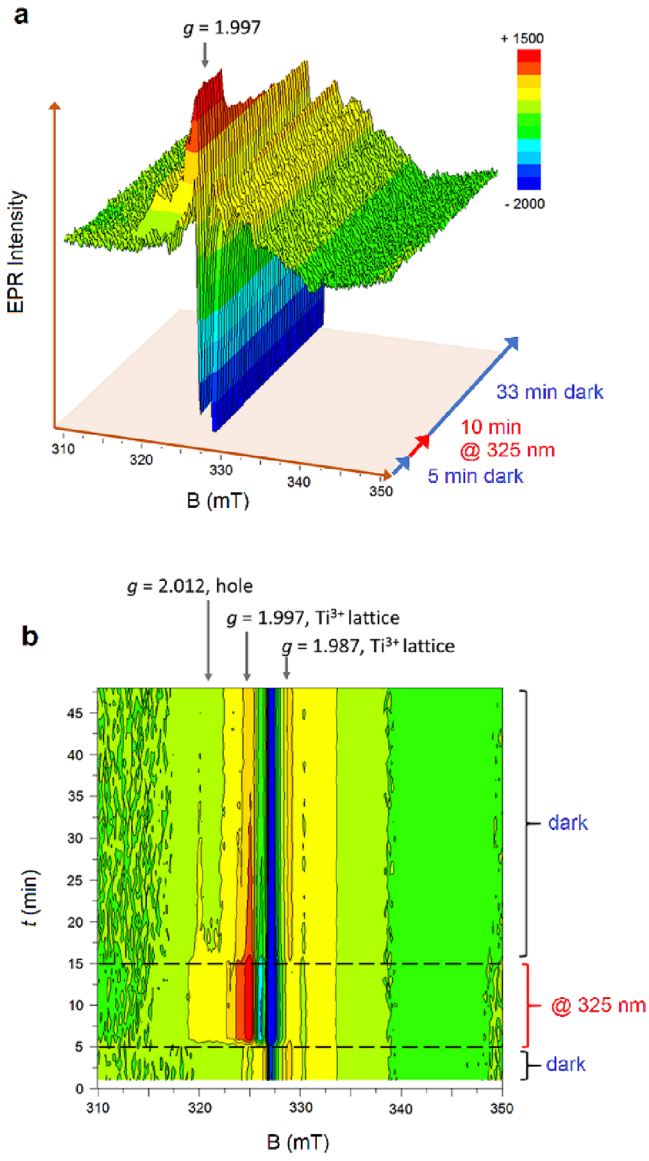

Figure 7. X-band LEPR spectra recorded at $T = 80$ K for *gray* TiO_2 nanoparticles dispersed in $NiSO_4$ solution (20 vol % $MeOH/H_2O$, nitrogen saturated), with and without light irradiation. Sequence: 5 min dark, 10 min UV, and 33 min dark. Experimental conditions: X-band frequency: 9.085 GHz, 1.6 mW applied power, 0.6 mT modulation width, 60 s sweep time for each sequential spectrum, and 0.03 s time constant.

if compared to that observed under UV light in the absence of hole scavenger (shown in Figure 6a−c). The spectra in Figure 7a,b also show a small increment in the amount of surface exposed Ti^{3+} sites under UV light. As soon as the UV light is switched off (from $t = 16$ to 48 min), the signal at $g = 2.012$ slowly decreases (the hole centers), and so does the signal at $g = 1.997$. The signal at $g = 1.987$ (Ti^{3+}) reforms while the excess of surface exposed Ti^{3+} sites generated under irradiation appears to slowly decrease over time.

By comparing the *in situ* EPR findings with the results of the photocatalytic experiments (Figure 1), and by considering the experimental differences between the photocatalytic and *in situ* EPR set-ups (temperature, illumination), we deduce that the activation toward H_2 evolution occurs by a combination of a fast and a slow process. The fast process is the formation of

https://doi.org/10.1021/jacs.3c08199
J. Am. Chem. Soc. 2023, 145, 26122−26132

metastable Ni^{+}-gray titania complex, while the slow process is a reorganization of the Ti^{3+} defect centers.[46] Hence, the ability of *gray* titania to evolve H_2 in the absence of hole scavenger can be linked to the formation of Ni^{+}-TiO_2−Ti^{3+} sites; notably, and as shown in the *in situ* EPR spectra in Figure S12 (see inset), such active state is only metastable, i.e., when the sample is exposed to ambient conditions (room temperature, UV light switched off), the distribution of spin species formed under light (active state) relaxes back to the starting distribution seen under dark conditions (resting state), and H_2 evolution ceases. In other words, the active form of the catalyst (Ni(I)-TiO_{2-x}) is present as such only in operando, and it returns to a state close to the initial situation, i.e., inactive, once the light is switched off.

In previous work,[46] *in situ* EPR experiments showed that illumination of *gray* titania for several days in plain H_2O in the absence of Ni^{2+} leads to a significant increase in the $g_{avg} \approx 1.93$ signature, i.e., a strong increase in the amount of Ti^{3+} surface states occurs in the absence of Ni^{2+}. This happens because swift electron transfer (to Ni cations in the solution) is not provided. In other words, TiO_2 conduction band electrons are not transferred to the environment, and hence undergo trapping at Ti^{3+} surface states. In contrast, in the presence of Ni^{2+}, even after 7 days of illumination, the intensity of the EPR signal at $g_{avg} \approx 1.92$ remains almost unaltered. In other words, in the absence of Ni^{2+} in solution, under illumination, electron accumulation takes place, leading to a steady self-reduction of the *gray* anatase. In the presence of Ni^{2+}, the electron transfer to the electrolyte (via the Ni^{+} surface relay) is sufficiently fast that self-reduction is limited.

On the other hand, the important role of *gray* titania as hole transfer mediator[4] is herein illustrated by comparing the behavior of *white* versus *gray* TiO_2 in Ni^{2+}-containing solutions in the absence or presence of methanol. In contrast to the inactive white form, *Gray* TiO_2 in 0.4 mM $NiSO_4$ aqueous solution not only evolves H_2 (via e^{-}_{CB} transfer to water) but also generates H_2O_2 after prolonged UV illumination (via h^{+}_{VB} transfer to water, see H_2O_2 strip test in Figure S10). Instead, *white* TiO_2 is found to evolve H_2 from Ni^{2+}-containing solutions only in the presence of MeOH (Figure 8); here, under illumination, methanol acts as the hole capturing agent, and hole-transfer is, thus, no longer the limiting factor. Note that in this case, H_2 evolution takes place with *gray* and *white* TiO_2 at comparable rate.

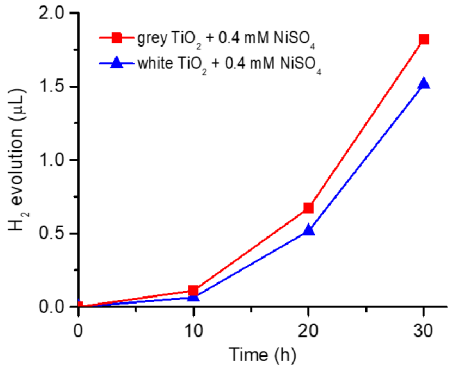

Figure 8. Comparison of H_2 production rates of *gray* TiO_2 nanoparticles vs *white* anatase TiO_2 nanoparticles in a 0.4 mM $NiSO_4$ methanol−water solution (50 vol % MeOH) under UV light irradiation (365 nm LED, 100 mW cm^{-2}).

CONCLUSIONS

In summary, in this work we demonstrated the light-induced self-assembly of a $Ni^{+}/TiO_2/Ti^{3+}$ photocatalyst that is active for H_2 generation from water in the absence of hole scavengers, e.g., methanol. This catalyst forms *in situ* when illuminating a suspension of reduced (*gray*) titania in a Ni^{2+} aqueous solution. No deposition of metallic Ni cocatalytic nanoparticles could be observed. Instead, we show that key to self-activation toward H_2 evolution is the formation of monovalent Ni^{+} species on the TiO_2 surface, combined with a light-induced rearrangement of defects in the semiconductor over time. Due to the metastable nature of the $Ni^{+}/TiO_2/Ti^{3+}$ photocatalyst, *in situ* techniques (XAS and EPR) were used to prove the formation of monovalent Ni^{+} and the occurrence of defect reorganization. These self-assembly and activation processes enabling H_2 evolution can be observed only for *gray* titania (and not for *white* or for *black* TiO_2), as only *gray* titania provides surface Ti^{3+}-O_V states with adequate energy to form active, metastable monovalent nickel species. *Gray* titania, in addition, provides the ability to transfer photoholes to plain water.

In a wider context, the present work demonstrates a self-assembly process where illumination is the synthesis tool for an active metastable entity, as well as the energy provider for this entity to achieve photocatalytic H_2 evolution from water. Self-amplifying reaction schemes as observed in the present work may have considerable potential for simple one-pot synthesis and use of photocatalysts.

ASSOCIATED CONTENT

Supporting Information

The Supporting Information is available free of charge at https://pubs.acs.org/doi/10.1021/jacs.3c08199.

Methods; additional SEM, XRD, photocatalytic, XPS, cyclic voltammetry, XAS, H_2O_2 test strips, and EPR data; in situ XAS setup pictures; additional references (PDF)

AUTHOR INFORMATION

Corresponding Authors

Marco Altomare − *PhotoCatalytic Synthesis PCS Group, MESA+ Institute for Nanotechnology, University of Twente, Enschede 7500 AE, The Netherlands;* orcid.org/0000-0002-7237-8809; Email: m.altomare@utwente.nl

Patrik Schmuki − *Department Materials Science WW-4, LKO, Friedrich-Alexander-University of Erlangen-Nuremberg (FAU), Erlangen 91058, Germany; Regional Centre of Advanced Technologies and Materials, Czech Advanced Technology and Research Institute, Palacký University Olomouc, Olomouc 779 00, Czech Republic;* orcid.org/0000-0002-9208-5771; Email: schmuki@ww.uni-erlangen.de

Authors

Shanshan Qin − *Department Materials Science WW-4, LKO, Friedrich-Alexander-University of Erlangen-Nuremberg (FAU), Erlangen 91058, Germany;* orcid.org/0000-0001-7693-115X

Viktoriia A. Saveleva − *ESRF, The European Synchrotron, Grenoble Cedex 9 38043, France*

Zdenek Badura − *Regional Centre of Advanced Technologies and Materials, Czech Advanced Technology and Research Institute, Palacký University Olomouc, Olomouc 779 00, Czech Republic; Nanotechnology Centre, VŠB − Technical*

University of Ostrava, Ostrava-Poruba 708 00, Czech Republic

Ondrej Tomanec − *Regional Centre of Advanced Technologies and Materials, Czech Advanced Technology and Research Institute, Palacký University Olomouc, Olomouc 779 00, Czech Republic*

Anca Mazare − *Department Materials Science WW-4, LKO, Friedrich-Alexander-University of Erlangen-Nuremberg (FAU), Erlangen 91058, Germany*

Giorgio Zoppellaro − *Regional Centre of Advanced Technologies and Materials, Czech Advanced Technology and Research Institute, Palacký University Olomouc, Olomouc 779 00, Czech Republic; Nanotechnology Centre, VŠB − Technical University of Ostrava, Ostrava-Poruba 708 00, Czech Republic*

Alberto Vertova − *Dipartimento di Chimica, Università degli Studi di Milano, Milan 20133, Italy;* orcid.org/0000-0003-3858-9730

Angelo Taglietti − *Dipartimento di Chimica, Università degli Studi di Pavia, Pavia 27100, Italy;* orcid.org/0000-0003-0141-9201

Alessandro Minguzzi − *Dipartimento di Chimica, Università degli Studi di Milano, Milan 20133, Italy;* orcid.org/0000-0002-8130-4465

Paolo Ghigna − *Dipartimento di Chimica, Università degli Studi di Pavia, Pavia 27100, Italy;* orcid.org/0000-0002-8680-7272

Complete contact information is available at: https://pubs.acs.org/10.1021/jacs.3c08199

Author Contributions

All authors contributed equally.

Notes

The authors declare no competing financial interest.

■ ACKNOWLEDGMENTS

The authors would like to acknowledge DFG and the Operational Program Research, Development and Education (European Regional Development Fund, project no. CZ.02.1.01/0.0/0.0/15_003/0000416 of the Ministry of Education, Youth and Sports of the Czech Republic) for financial support. We acknowledge the European Synchrotron Radiation Facility for provision of beamtime at ID26 beamline (DOI: 10.15151/ESRF-ES-561460108). M.A. acknowledges the Deutsche Forschungsgemeinschaft DFG (project no. DFG-grant AL 2479/1-1 30965319) and the Nederlandse Organisatie voor Wetenschappelijk Onderzoek NWO (project no. ECCM.TT.ECCM.005) for financial support. G.Z. and Z.B. acknowledge the project APPROACH No 101120397, HORIZON-WIDERA-2022-TALENTS, and the European Union under the REFRESH - Research Excellence For Region Sustainability and High-tech Industries project number CZ.10.03.01/00/22_003/0000048 via the Operational Programme Just Transition.

■ REFERENCES

(1) Whitesides, G. M.; Grzybowski, B. Self-Assembly at All Scales. *Science* **2002**, *295*, 2418−2421.

(2) Eigen, M. Selforganization of matter and the evolution of biological macromolecules. *Naturwissenschaften* **1971**, *58*, 465−523.

(3) Zhang, J.; Nosaka, Y. Mechanism of the OH Radical Generation in Photocatalysis with TiO_2 of Different Crystalline Types. *J. Phys. Chem. C* **2014**, *118*, 10824−10832.

(4) Liu, N.; Mohajernia, S.; Nguyen, N. T.; Hejazi, S.; Plass, F.; Kahnt, A.; Yokosawa, T.; Osvet, A.; Spiecker, E.; Guldi, D. M.; et al. Long-Living Holes in Grey Anatase TiO_2 Enable Noble-Metal-Free and Sacrificial-Agent-Free Water Splitting. *ChemSusChem* **2020**, *13*, 4937−4944.

(5) Nosaka, Y.; Nosaka, A. Understanding Hydroxyl Radical (•OH) Generation Processes in Photocatalysis. *ACS Energy Lett.* **2016**, *1*, 356−359.

(6) Diesen, V.; Jonsson, M. Formation of H_2O_2 in TiO_2 Photocatalysis of Oxygenated and Deoxygenated Aqueous Systems: A Probe for Photocatalytically Produced Hydroxyl Radicals. *J. Phys. Chem. C* **2014**, *118*, 10083−10087.

(7) Ge, M.; Cai, J.; Iocozzia, J.; Cao, C.; Huang, J.; Zhang, X.; Shen, J.; Wang, S.; Zhang, S.; Zhang, K.-Q.; et al. A review of TiO_2 nanostructured catalysts for sustainable H_2 generation. *Int. J. Hydrogen Energy* **2017**, *42*, 8418−8449.

(8) Ni, M.; Leung, M. K. H.; Leung, D. Y. C.; Sumathy, K. A review and recent developments in photocatalytic water-splitting using TiO_2 for hydrogen production. *Renewable and Sustainable Energy Rev.* **2007**, *11*, 401−425.

(9) Nakata, K.; Fujishima, A. TiO_2 photocatalysis: Design and applications. *J. Photochem. Photobiol., C* **2012**, *13*, 169−189. Osterloh, F. E. Inorganic Materials as Catalysts for Photochemical Splitting of Water. *Chem. Mater.* **2008**, *20* (1), 35−54.

(10) Kudo, A.; Miseki, Y. Heterogeneous photocatalyst materials for water splitting. *Chem. Soc. Rev.* **2009**, *38*, 253−278.

(11) Fujishima, A.; Zhang, X.; Tryk, D. A. TiO_2 photocatalysis and related surface phenomena. *Surf. Sci. Rep.* **2008**, *63*, 515−582.

(12) Schneider, J.; Matsuoka, M.; Takeuchi, M.; Zhang, J.; Horiuchi, Y.; Anpo, M.; Bahnemann, D. W. Understanding TiO_2 Photocatalysis: Mechanisms and Materials. *Chem. Rev.* **2014**, *114*, 9919−9986.

(13) Chen, S.; Takata, T.; Domen, K. Particulate photocatalysts for overall water splitting. *Nat. Rev. Mater.* **2017**, *2*, 17050.

(14) Yoshida, M.; Yamakata, A.; Takanabe, K.; Kubota, J.; Osawa, M.; Domen, K. ATR-SEIRAS Investigation of the Fermi Level of Pt Cocatalyst on a GaN Photocatalyst for Hydrogen Evolution under Irradiation. *J. Am. Chem. Soc.* **2009**, *131*, 13218−13219.

(15) Maeda, K.; Teramura, K.; Lu, D.; Saito, N.; Inoue, Y.; Domen, K. Noble-Metal/Cr_2O_3 Core/Shell Nanoparticles as a Cocatalyst for Photocatalytic Overall Water Splitting. *Angew. Chem., Int. Ed.* **2006**, *45*, 7806−7809.

(16) Gomes Silva, C.; Juárez, R.; Marino, T.; Molinari, R.; García, H. Influence of Excitation Wavelength (UV or Visible Light) on the Photocatalytic Activity of Titania Containing Gold Nanoparticles for the Generation of Hydrogen or Oxygen from Water. *J. Am. Chem. Soc.* **2011**, *133*, 595−602.

(17) Chen, X.; Shen, S.; Guo, L.; Mao, S. S. Semiconductor-based Photocatalytic Hydrogen Generation. *Chem. Rev.* **2010**, *110*, 6503−6570.

(18) Wang, Q.; Domen, K. Particulate Photocatalysts for Light-Driven Water Splitting: Mechanisms, Challenges, and Design Strategies. *Chem. Rev.* **2020**, *120*, 919−985.

(19) Kamat, P. V.; Jin, S. Semiconductor Photocatalysis: "*Tell Us the Complete Story!*". *ACS Energy Lett.* **2018**, *3*, 622−623.

(20) Schneider, J.; Bahnemann, D. W. Undesired Role of Sacrificial Reagents in Photocatalysis. *J. Phys. Chem. Lett.* **2013**, *4*, 3479−3483.

(21) Yuan, J.; Wen, J.; Zhong, Y.; Li, X.; Fang, Y.; Zhang, S.; Liu, W. Enhanced photocatalytic H_2 evolution over noble-metal-free NiS cocatalyst modified CdS nanorods/g-C_3N_4 heterojunctions. *J. Mater. Chem. A* **2015**, *3*, 18244−18255.

(22) Zong, X.; Han, J.; Ma, G.; Yan, H.; Wu, G.; Li, C. Photocatalytic H_2 Evolution on CdS Loaded with WS_2 as Cocatalyst under Visible Light Irradiation. *J. Phys. Chem. C* **2011**, *115*, 12202−12208.

(23) Sun, Z.; Zheng, H.; Li, J.; Du, P. Extraordinarily efficient photocatalytic hydrogen evolution in water using semiconductor nanorods integrated with crystalline Ni_2P cocatalysts. *Energy Environ. Sci.* **2015**, *8*, 2668−2676.

(24) Zong, X.; Yan, H.; Wu, G.; Ma, G.; Wen, F.; Wang, L.; Li, C. Enhancement of Photocatalytic H_2 Evolution on CdS by Loading MoS_2

as Cocatalyst under Visible Light Irradiation. *J. Am. Chem. Soc.* **2008**, *130*, 7176−7177.
(25) Zhang, X.; Fu, A.; Chen, X.; Liu, L.; Ren, L.; Tong, L.; Ye, J. Highly efficient Cu induced photocatalysis for visible-light hydrogen evolution. *Catal. Today* **2019**, *335*, 166−172.
(26) Peng, Y.; Jiang, K.; Hill, W.; Lu, Z.; Yao, H.; Wang, H. Large-Scale, Low-Cost, and High-Efficiency Water-Splitting System for Clean H_2 Generation. *ACS Appl. Mater. Interfaces* **2019**, *11*, 3971−3977.
(27) Spanu, D.; Recchia, S.; Mohajernia, S.; Tomanec, O.; Kment, Š.; Zboril, R.; Schmuki, P.; Altomare, M. Templated Dewetting−Alloying of NiCu Bilayers on TiO_2 Nanotubes Enables Efficient Noble-Metal-Free Photocatalytic H_2 Evolution. *ACS Catal.* **2018**, *8*, 5298−5305.
(28) Shahvaranfard, F.; Ghigna, P.; Minguzzi, A.; Wierzbicka, E.; Schmuki, P.; Altomare, M. Dewetting of PtCu Nanoalloys on TiO_2 Nanocavities Provides a Synergistic Photocatalytic Enhancement for Efficient H_2 Evolution. *ACS Appl. Mater. Interfaces* **2020**, *12*, 38211−38221.
(29) Pinna, M.; Wei, A. W. W.; Spanu, D.; Will, J.; Yokosawa, T.; Spiecker, E.; Recchia, S.; Schmuki, P.; Altomare, M. Amorphous NiCu Thin Films Sputtered on TiO_2 Nanotube Arrays: A Noble-Metal Free Photocatalyst for Hydrogen Evolution. *ChemCatChem* **2022**, *14*, No. e202201052.
(30) Chen, W.-T.; Chan, A.; Sun-Waterhouse, D.; Llorca, J.; Idriss, H.; Waterhouse, G. I. N. Performance comparison of Ni/TiO_2 and Au/TiO_2 photocatalysts for H_2 production in different alcohol-water mixtures. *J. Catal.* **2018**, *367*, 27−42.
(31) Melián, E. P.; Suárez, M. N.; Jardiel, T.; Rodríguez, J. M. D.; Caballero, A. C.; Araña, J.; Calatayud, D. G.; Díaz, O. G. Influence of nickel in the hydrogen production activity of TiO_2. *Appl. Catal., B* **2014**, *152*−*153*, 192−201.
(32) Xu, Y.; Xu, R. Nickel-based cocatalysts for photocatalytic hydrogen production. *Appl. Surf. Sci.* **2015**, *351*, 779−793.
(33) Chen, W.-T.; Chan, A.; Sun-Waterhouse, D.; Moriga, T.; Idriss, H.; Waterhouse, G. I. N. Ni/TiO_2: A promising low-cost photocatalytic system for solar H_2 production from ethanol−water mixtures. *J. Catal.* **2015**, *326*, 43−53.
(34) Wang, J.; Mao, S.; Liu, Z.; Wei, Z.; Wang, H.; Chen, Y.; Wang, Y. Dominating Role of Ni^0 on the Interface of Ni/NiO for Enhanced Hydrogen Evolution Reaction. *ACS Appl. Mater. Interfaces* **2017**, *9*, 7139−7147.
(35) Townsend, T. K.; Browning, N. D.; Osterloh, F. E. Overall photocatalytic water splitting with NiO_x−$SrTiO_3$ − a revised mechanism. *Energy Environ. Sci.* **2012**, *5*, 9543−9550.
(36) Wang, W.; Liu, S.; Nie, L.; Cheng, B.; Yu, J. Enhanced photocatalytic H_2-production activity of TiO_2 using $Ni(NO_3)_2$ as an additive. *Phys. Chem. Chem. Phys.* **2013**, *15*, 12033−12039.
(37) Forouzan, F.; Richards, T. C.; Bard, A. J. Photoinduced Reaction at TiO_2 Particles. Photodeposition from Ni^{II} Solutions with Oxalate. *J. Chem. Phys.* **1996**, *100*, 18123−18127.
(38) Spanu, D.; Minguzzi, A.; Recchia, S.; Shahvardanfard, F.; Tomanec, O.; Zboril, R.; Schmuki, P.; Ghigna, P.; Altomare, M. An Operando X-ray Absorption Spectroscopy Study of a NiCu−TiO_2 Photocatalyst for H_2 Evolution. *ACS Catal.* **2020**, *10*, 8293−8302.
(39) Han, K.; Kreuger, T.; Mei, B.; Mul, G. Transient Behavior of Ni@NiO_x Functionalized $SrTiO_3$ in Overall Water Splitting. *ACS Catal.* **2017**, *7*, 1610−1614.
(40) Nosaka, Y.; Nosaka, A. Y. Generation and Detection of Reactive Oxygen Species in Photocatalysis. *Chem. Rev.* **2017**, *117*, 11302−11336.
(41) Kiwi, J.; Graetzel, M. Optimization of conditions for photochemical water cleavage. Aqueous platinum/TiO_2 (anatase) dispersions under ultraviolet light. *J. Chem. Phys.* **1984**, *88*, 1302−1307.
(42) Kiwi, J.; Graetzel, M. Specific analysis of surface-bound peroxides formed during photoinduced water cleavage in titanium dioxide-based microheterogeneous systems. *J. Mol. Catal.* **1987**, *39*, 63−70.
(43) Munuera, G.; Espinós, J. P.; Fernández, A.; Malet, P.; González-Elipe, A. R. TiO_2 corrosion during water photocleavage using Rh/TiO_2 suspensions. *J. Chem. Soc., Faraday Trans.* **1990**, *86*, 3441−3445.
(44) Siahrostami, S.; Li, G.-L.; Viswanathan, V.; Nørskov, J. K. One- or Two-Electron Water Oxidation, Hydroxyl Radical, or H_2O_2 Evolution. *J. Phys. Chem. Lett.* **2017**, *8*, 1157−1160.
(45) Liu, N.; Zhou, X.; Nguyen, N. T.; Peters, K.; Zoller, F.; Hwang, I.; Schneider, C.; Miehlich, M. E.; Freitag, D.; Meyer, K.; et al. Black Magic in Gray Titania: Noble-Metal-Free Photocatalytic H_2 Evolution from Hydrogenated Anatase. *ChemSusChem* **2017**, *10*, 62−67.
(46) Qin, S.; Badura, Z.; Denisov, N.; Tomanec, O.; Mohajernia, S.; Liu, N.; Kment, S.; Zoppellaro, G.; Schmuki, P. Self-assembly of a Ni(I)-photocatalyst for plain water splitting without sacrificial agents. *Electrochem. Commun.* **2021**, *122*, 106909.
(47) Chen, X.; Liu, L.; Yu, P. Y.; Mao, S. S. Increasing Solar Absorption for Photocatalysis with Black Hydrogenated Titanium Dioxide Nanocrystals. *Science* **2011**, *331*, 746−750.
(48) Chen, X.; Liu, L.; Huang, F. Black titanium dioxide (TiO_2) nanomaterials. *Chem. Soc. Rev.* **2015**, *44*, 1861−1885.
(49) Liu, N.; Schneider, C.; Freitag, D.; Hartmann, M.; Venkatesan, U.; Müller, J.; Spiecker, E.; Schmuki, P. Black TiO_2 Nanotubes: Cocatalyst-Free Open-Circuit Hydrogen Generation. *Nano Lett.* **2014**, *14*, 3309−3313.
(50) Naldoni, A.; Altomare, M.; Zoppellaro, G.; Liu, N.; Kment, Š; Zbořil, R.; Schmuki, P. Photocatalysis with Reduced TiO_2: From Black TiO_2 to Cocatalyst-Free Hydrogen Production. *ACS Catal.* **2019**, *9*, 345−364.
(51) Wierzbicka, E.; Altomare, M.; Wu, M.; Liu, N.; Yokosawa, T.; Fehn, D.; Qin, S.; Meyer, K.; Unruh, T.; Spiecker, E.; et al. Reduced grey brookite for noble metal free photocatalytic H_2 evolution. *J. Mater. Chem. A* **2021**, *9*, 1168−1179.
(52) Will, J.; Wierzbicka, E.; Wu, M.; Götz, K.; Yokosawa, T.; Liu, N.; Tesler, A. B.; Stiller, M.; Unruh, T.; Altomare, M.; et al. Hydrogenated anatase TiO_2 single crystals: Defects formation and structural changes as microscopic origin of co-catalyst free photocatalytic H_2 evolution activity. *J. Mater. Chem. A* **2021**, *9*, 24932−24942.
(53) Qin, S.; Kim, H.; Denisov, N.; Fehn, D.; Schmidt, J.; Meyer, K.; Schmuki, P. Grey facet-controlled anatase nanosheets for photocatalytic H_2 evolution without co-catalyst. *J. Phys.: Energy* **2021**, *3*, 034003.
(54) Liu, N.; Schneider, C.; Freitag, D.; Venkatesan, U.; Marthala, V. R. R.; Hartmann, M.; Winter, B.; Spiecker, E.; Osvet, A.; Zolnhofer, E. M.; et al. Hydrogenated Anatase: Strong Photocatalytic Dihydrogen Evolution without the Use of a Co-Catalyst. *Angew. Chem., Int. Ed.* **2014**, *53*, 14201−14205.
(55) Mohajernia, S.; Andryskova, P.; Zoppellaro, G.; Hejazi, S.; Kment, S.; Zboril, R.; Schmidt, J.; Schmuki, P. Influence of Ti^{3+} defect-type on heterogeneous photocatalytic H_2 evolution activity of TiO_2. *J. Mater. Chem. A* **2020**, *8*, 1432−1442.
(56) Qin, S.; Denisov, N.; Zhou, X.; Zdražil, L.; Fehn, D.; Hwang, I.; Bruns, M.; Kim, H.; Meyer, K.; Schmuki, P. Critical factors for photoelectrochemical and photocatalytic H_2 evolution from gray anatase (001) nanosheets. *J. Phys.: Energy* **2022**, *4*, 044004.
(57) Wierzbicka, E.; Zhou, X.; Denisov, N.; Yoo, J.; Fehn, D.; Liu, N.; Meyer, K.; Schmuki, P. Self-Enhancing H_2 Evolution from TiO_2 Nanostructures under Illumination. *ChemSusChem* **2019**, *12*, 1900−1905.
(58) Lo, W. J.; Chung, Y. W.; Somorjai, G. A. Electron spectroscopy studies of the chemisorption of O_2, H_2 and H_2O on the TiO_2(100) surfaces with varied stoichiometry: Evidence for the photogeneration of Ti^{+3} and for its importance in chemisorption. *Surf. Sci.* **1978**, *71*, 199−219.
(59) Millet, M.-M.; Algara-Siller, G.; Wrabetz, S.; Mazheika, A.; Girgsdies, F.; Teschner, D.; Seitz, F.; Tarasov, A.; Levchenko, S. V.; Schlögl, R.; et al. Ni Single Atom Catalysts for CO_2 Activation. *J. Am. Chem. Soc.* **2019**, *141*, 2451−2461.
(60) Wang, A.; Li, J.; Zhang, T. Heterogeneous single-atom catalysis. *Nat. Rev. Chem.* **2018**, *2*, 65−81.
(61) Gao, C.; Low, J.; Long, R.; Kong, T.; Zhu, J.; Xiong, Y. Heterogeneous Single-Atom Photocatalysts: Fundamentals and Applications. *Chem. Rev.* **2020**, *120*, 12175−12216.

(62) Moulder, J. F.; Stickle, W. F.; Sobol, P. E.; Bomben, K. D.. *Handbook of X-ray Photoelectron Spectroscopy*; Perkin Elmer Corp.,: Eden Prairie/USA, 1992.
(63) Grosvenor, A. P.; Biesinger, M. C.; Smart, R. S. C.; McIntyre, N. S. New interpretations of XPS spectra of nickel metal and oxides. *Surf. Sci.* **2006**, *600*, 1771−1779.
(64) Biesinger, M. C.; Payne, B. P.; Lau, L. W. M.; Gerson, A.; Smart, R. S. C. X-ray photoelectron spectroscopic chemical state quantification of mixed nickel metal, oxide and hydroxide systems. *Surf. Interface Anal.* **2009**, *41*, 324−332.
(65) Dubey, P.; Kaurav, N.; Devan, R. S.; Okram, G. S.; Kuo, Y. K. The effect of stoichiometry on the structural, thermal and electronic properties of thermally decomposed nickel oxide. *RSC Adv.* **2018**, *8*, 5882−5890.
(66) Nesbitt, H. W.; Legrand, D.; Bancroft, G. M. Interpretation of Ni2p XPS spectra of Ni conductors and Ni insulators. *Phys. Chem. Miner.* **2000**, *27*, 357−366.
(67) Abba, F.; De Santis, G.; Fabbrizzi, L.; Licchelli, M.; Manotti Lanfredi, A. M.; Pallavicini, P.; Poggi, A.; Ugozzoli, F. Nickel(II) Complexes of Azacyclams: Oxidation and Reduction Behavior and Catalytic Effects in the Electroreduction of Carbon Dioxide. *Inorg. Chem.* **1994**, *33*, 1366−1375.
(68) Di Casa, M.; Fabbrizzi, L.; Licchelli, M.; Poggi, A.; Sacchi, D.; Zema, M. A novel fluorescence redox switch based on the formal Ni^{II}/Ni^{I} couple. *J. Chem. Soc., Dalton Trans.* **2001**, 1671−1675.
(69) Lovecchio, F. V.; Gore, E. S.; Busch, D. H. Oxidation and reduction behavior of macrocyclic complexes of nickel. Electrochemical and electron spin resonance studies. *J. Am. Chem. Soc.* **1974**, *96*, 3109−3118.
(70) Bad'ura, Z.; Naldoni, A.; Qin, S.; Bakandritsos, A.; Kment, Š.; Schmuki, P.; Zoppellaro, G. Light-Induced Migration of Spin Defects in TiO_2 Nanosystems and their Contribution to the H_2 Evolution Catalysis from Water. *ChemSusChem* **2021**, *14*, 4408−4414.

https://doi.org/10.1021/jacs.3c08199
J. Am. Chem. Soc. 2023, 145, 26122−26132